Vibrational Strong Coupling of Thin Water Layers Using Plasmonic Cavities

*Jyoti Lather, Rohit B. Raj, Nikolai Orlov, Devin B. O'Neill, Elaina Galvin, Christoph Kaiser, Huib J. Bakker, and Erik C. Garnett**

Strong coupling of molecular vibrations with resonant optical cavities creates vibro-polaritonic states, which can alter chemical reaction rates and product distributions without altering molecular structure. However, so far vibrational strong coupling has only been demonstrated in films of material so thick that the effects have been limited to bulk chemical reactions. Demonstrating vibrational strong coupling in nanometer-scale surface layers of molecules facilitates applying the results of vibro-polaritonic chemistry to the vast majority of industrial chemistry: catalytic reactions occurring at surfaces. Here, highly confined plasmonic cavities are designed and fabricated that are tunable over the entire mid-infrared region. Vibrational strong coupling of water layers that are only 44 nm thick, in both the O—H stretching and bending modes is demonstrated, with Rabi splitting energy of 468 and 282 cm^{-1}, respectively. Detuning experiments show the dispersive behavior of the polaritonic states, and changing the oscillator strength of water molecules by diluting with D_2O follows the theoretically predicted change in Rabi splitting energy, assuming a strongly bound layer of water at the surface. We confirm that dry samples annealed in vacuum and measured under nitrogen purging still display a substantial Rabi splitting of 202 cm^{-1} coming from surface-bound water with an estimated thickness from literature of a few monolayers to a few nanometers, closely approaching the 242 cm^{-1} threshold for vibrational strong coupling. Such strongly perturbed water layers directly at the surface of metal electrodes broaden the relevant range of reactions where vibro-polaritonic chemistry can be applied and point toward the exciting possibility of a totally new way of altering aqueous electrocatalytic activity for important reactions such as water-splitting and CO_2 reduction.

1. Introduction

Over the last decade, vibrational strong coupling (VSC) has pointed toward a unique approach for modulating chemical and material properties.[1–4] By placing molecules or materials in optical cavities tuned to relevant vibrational modes, VSC can be used to create new hybrid light-matter states that control reaction pathways, enhancing or suppressing the reactivity, product selectivity, ionic conductivity, crystallization, and even the catalytic activity of enzymes.[5–11] Vibrational strong coupling occurs when the energy exchange between an optical cavity and a vibrational mode is faster than the relaxation rate of either uncoupled excited state. In analogy to chemical bonding, this strong coupling leads to two new hybrid states known as the upper and lower vibro-polaritonic states, which also show different behavior from the original states.[12,13] The energy separating these new hybrid states is known as the vacuum Rabi splitting energy ($\hbar\Omega_{VR}$). In further analogy with bonding states, the hybrid vibro-polaritonic states also exist in the dark (no pumping of the optical cavity), which has led to the ability to change chemical reactivity simply by placing molecules in a resonant optical cavity in the dark, for example between two mirrors (Fabry–Perot cavity).[14] In addition to providing energy level matching, this cavity also must provide sufficient coupling between the optical mode and the molecular vibrational mode. This coupling can be enhanced by increasing the number of molecules interacting with the cavity and by increasing the interaction per molecule. Most VSC experiments are performed in Fabry–Perot cavities, where two mirrors confine the optical resonance to a volume of $\approx\lambda^3$, where λ is the cavity photon energy resonant with molecular vibrations (several micron gap between mirrors).[15,16] The large mode volume and high cavity quality factor (many reflections between mirrors before photons decay) lead to excellent coupling, but also limit vibrational strong coupling to reactions occurring in bulk solution, while the vast majority of industrial reactions are catalyzed at surfaces. Looking toward the energy transition, the whole chemical industry will

---

J. Lather, R. B. Raj, N. Orlov, D. B. O'Neill, E. Galvin, C. Kaiser, H. J. Bakker
LMPV Sustainable Energy Materials
AMOLF
Science Park 104, Amsterdam 1098XG

**ADVANCED
SCIENCE NEWS**

www.advancedsciencenews.com

**ADVANCED
OPTICAL
MATERIALS**
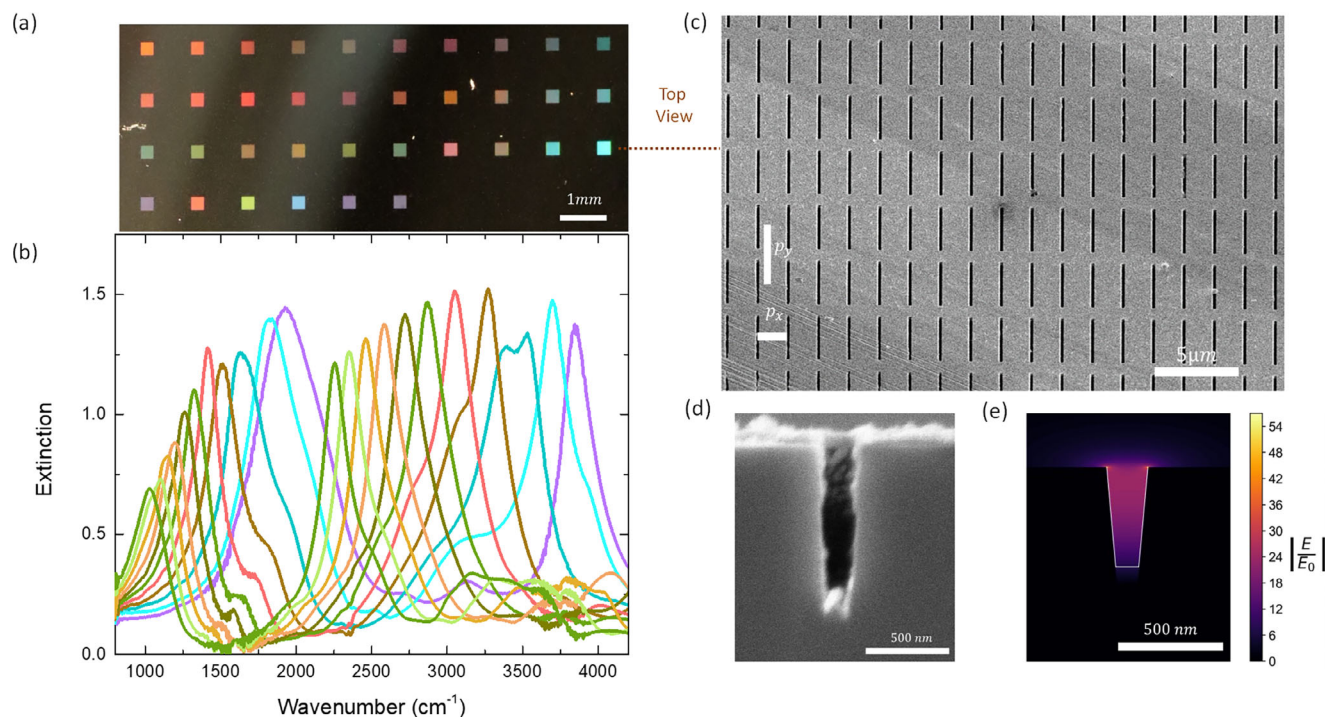
www.advopticalmat.de

Figure 1. Plasmonic cavities tunable in the mid-infrared region. a) picture of the fabricated sample that shows a different array with varying periodicity from P_x = 500 nm to 4000 nm and fixed P_y = 5000 nm. b) Short axis excitation gives the FTIR spectra of the plasmonic cavities and the mid-IR resonance tuned by varying the periodicity P_x (curve colors corresponds to the above array). c,d) SEM image of the fabricated grooves (c) top view of the sample (d) undercut image of the sample. e) FDTD-simulations for the field enhancement profile with the vertical monitor along the short axis of the nanogroove.

need to be transformed to run off green electricity, likely using electrochemical or electrothermal processes, which require metallic electrodes.[17] Plasmonic cavities provide extreme surface resonance confinement (typically 10's of nanometers) and can be patterned into continuous metal films, thereby satisfying the two conditions above, and offering an intriguing alternative to the traditional Fabry–Perot cavities for VSC.[18–23] However, the small number of molecules present within the optical mode and the typically lower quality factor for plasmonic cavities has limited VSC in plasmonic systems to films of material at least hundreds of nanometers thick, far beyond the scale relevant to influence surface-catalyzed reactions.[24–29] Here we show that 44 nm layers of water on the surface of nanogroove array plasmonic cavities can reach vibrational strong coupling, and even surface-adsorbed water from the atmosphere on dry cavities is on the threshold of strong coupling. VSC is achieved by exploiting the high quality factor present in lattice resonances, which boosts the interaction of the electromagnetic field with the surface water molecules, enhancing the coupling strength (g) such that it can exceed the average decay rate of the plasmonic cavity (κ) and molecular vibration (γ), $2g > \frac{\gamma + \kappa}{2}$. Experimentally, this condition corresponds to the peak splitting seen in infrared spectra (Ω_{VR}) exceeding the average linewidth of the uncoupled plasmonic and water vibrational resonances.[30] The extreme field confinement provided by the plasmonic cavities ensures that all strongly coupled water molecules are near the surface, where heterogeneous (electro)catalysis takes place, opening up the possibility of a new mechanism for tuning surface-catalyzed reactions.

2. Plasmonic Cavity Tunability in the Mid-Infrared Region

The plasmonic cavities are fabricated using electron beam lithography and deep reactive ion etching on a Si substrate, followed by physical vapor deposition of a silver film. Due to similar lattice constants between Si and Ag, it is possible to grow the silver as either a polycrystalline or monocrystalline film.[31] Details of the fabrication and characterization of the Ag film crystallinity are provided in (Sections S2 and S3, Supporting Information). **Figure 1c** shows the plan view scanning electron microscope (SEM) image of the groove array with a periodicity of P_x = 1400 nm and P_y = 5000 nm. Each array is fabricated to be 250 × 250 µm² to enable simple characterization with a Fourier transform infrared (FTIR) microscope. We optimize the array location with the 15× microscope objective (numerical aperture = 0.4, incident angle range ± 23.6°) on the FTIR using a standard visible light source. These nanogroove lattice optical modes were used because they show high field confinement, narrow linewidth, tunable peak position and superior coupling compared to particle-based plasmonic modes.[32] A polarizer is inserted into the beam path to polarize the light linearly with the electrical field vector along the short axis of the nanogrooves. We designed the groove arrays with different periodicity along the x direction varying from P_x = 500 to 4000 nm in increments of 100 nm, and fixed the periodicity in the y direction to P_y = 5000 nm. This lattice period variation enables tuning across the entire mid-IR spectral range, with also variations in visible optical resonance frequencies (Figure 1a). These plasmonic cavities display two major mid-IR modes. The
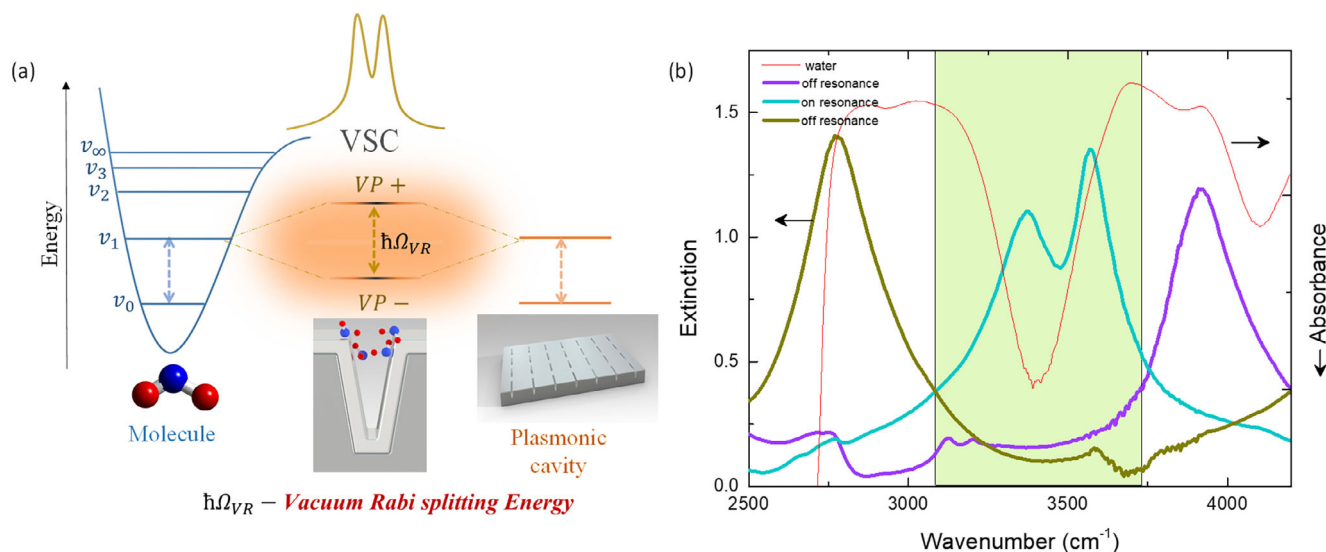
e01890 (2 of 7)

**ADVANCED
SCIENCE NEWS**

www.advancedsciencenews.com

**ADVANCED
OPTICAL
MATERIALS**

www.advopticalmat.de

Figure 2. a) Schematic of plasmonic coupling and Rabi splitting on dry plasmonic cavities. Mid-IR light is confined in an array of grooves that form the plasmonic cavity. The photonic resonance (orange dotted arrow) couples with the fundamental vibration of water molecules adsorbed on the dry surface from the atmosphere, (blue dotted arrow) that results in new hybrid photonic-vibrational states known as the upper polariton VP_+ and lower polariton VP_- (yellow curve) that are separated by the Rabi splitting energy ($\hbar\Omega_{VR}$)). b) Extinction spectra of a dry plasmonic cavity coupled On-resonance with the O—H stretching frequency of water molecules adsorbed on the surface which leads to a Rabi splitting of 202 cm^{-1} (cyan curve) and uncoupled off-resonant plasmonic modes (gold and purple curves) that show no peak splitting. The red curve shows the FTIR spectrum of 1% water diluted with D$_2$O solvent to facilitate visualizing the water peak in bulk solution without saturating the detector.

resonance tunability for the 1st mode (used to tune across the water bending) is from ≈1000 to 2500 cm^{-1}, and the 2nd mode (used to tune across the water stretching) is from ≈2000 to 4200 cm^{-1} (Figure 1b). Both modes demonstrate strong extinction, and the decay rate can be calculated using the linewidth of the modes, which varies from 240 to 660 cm^{-1}, depending on the periodicity. Finite difference time domain (FDTD) simulations are used to extract the near-field profile of the silver nanogroove array. The color map shows that the fields are confined predominantly in the center of the groove with the enhancement of E/E_0 ∼ 30 (Figure 1e, higher values up to 60 only appear at perfectly sharp corners that do not exist in the fabricated structures). The extinction spectra resulting from normal incidence excitation polarized along the short axis of the grooves, with the periodicity changing also in that direction, show that the resonance can be tuned across the entire mid-IR range. Additional simulations at different angles of incidence covering the relevant range for our FTIR microscope show that the peaks maintain the same spectral position, but broaden slightly at higher angles (Figure S1, Supporting Information). This angle-insensitivity provides another strong advantage for our system over the standard Fabry–Perot geometry, which suffers from severe angle dispersion.

3. Surface-Bound Water Molecules Approaching Vibrational Strong Coupling

Plasmonic cavities have been applied extensively in surface-enhanced infrared absorption spectroscopy (SEIRAS) to amplify and measure weak vibrational signals.[33] These nanogroove cavities are able to confine electromagnetic fields to the deeply sub-wavelength scale, greatly enhancing the infrared adsorption signals of molecules. In our case, we even see signals from the trace

CO$_2$ and H$_2$O adsorbed on the surface, which remains after nitrogen purging. This can be seen clearly by analyzing the extinction spectra of the bare nanogrooves, which show SEIRAS signal for the C—O asymmetric stretching band of CO$_2$ but no peak splitting as would be expected with strong coupling (Figure S4, Supporting Information). Interestingly, we found that water molecules adsorbed from the atmosphere do lead to peak splitting (**Figure 2b**). The origin of this effect is shown schematically in Figure 2a. When two oscillators couple together – one representing the fundamental molecular vibration and the other the mid-IR plasmonic mode – they form two new states of mixed character called polaritonic states, leading to the formation of a spectrum with two distinct peaks separated by the Rabi splitting energy. Focusing on the O—H stretching frequency of water at 3400 cm^{-1} (red curve in Figure 2b), the coupled resonance clearly splits into two new peaks, corresponding to the upper and lower polaritonic states (UP, LP) appearing in this case at 3572 and 3370 cm^{-1} (Figure 2b; cyan color spectrum). These two distinct polaritonic resonances are notably absent when moving the plasmonic resonance away from the water O—H stretching frequency band either at higher or lower frequencies, indicated by the purple and gold curves in Figure 2b (off resonance). The observed peak splitting corresponds to a Rabi splitting energy of $\hbar\Omega_{VR} = 202$ cm^{-1}, which is almost as large as the linewidth of the cavity mode (≈258 cm^{-1}) and the O—H stretching band of water (≈225 cm^{-1}), indicating that these polaritonic states have nearly reached vibrational strong coupling even with only water molecules adsorbed from the atmosphere. Since the peak splitting remained present even under nitrogen purging and after vacuum annealing, we expect the water layer to be between a few monolayers and a few nanometers, since even at 15–25% relative humidity, adsorbed water on gold was shown to be only
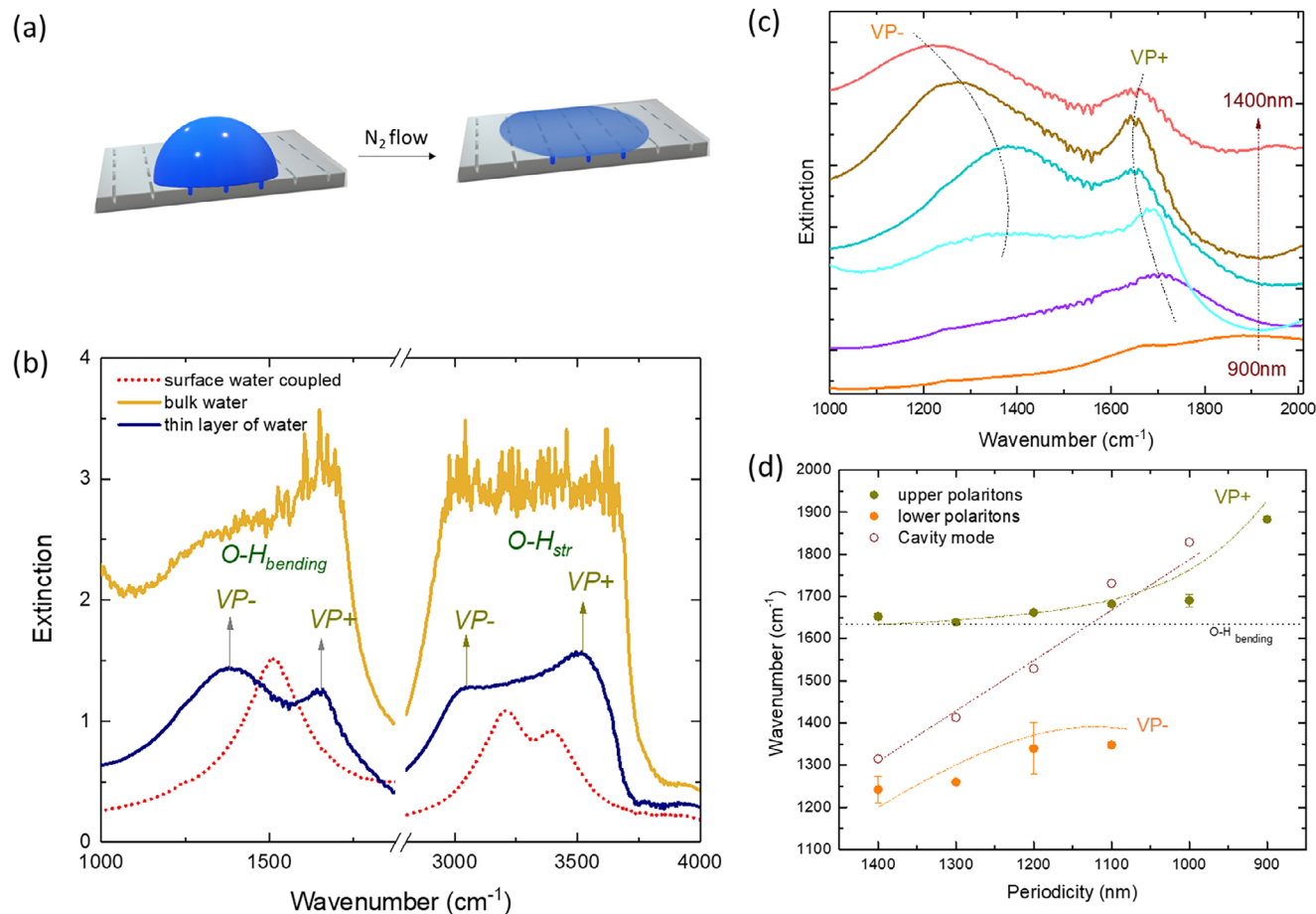
e01890 (3 of 7)

ADVANCED
SCIENCE NEWS

www.advancedsciencenews.com

ADVANCED
OPTICAL
MATERIALS

www.advopticalmat.de

Figure 3. a) Illustration of adding water molecules in the cavities and purge the N_2 in the chamber until the a thin layer of water formed. b) Probing the extinction spectra from bulk water (yellow curve) to the formation of a thin water layer (blue curve). FTIR spectra show that the bare plasmonic mode is ON-resonance for O—H$_{str}$ and O—H$_{bend}$ (dashed red curve), adding bulk water (yellow curve), a thin layer of water that shows a new polaritonic peak appears, representing as VP_+ and VP_- for the O—H$_{bend}$ as well as O2500H$_{str}$ (blue curve). c) Shifting of polaritonic peaks VP_+ and VP_- with changing the plasmonic mode positions for detuning of O—H$_{bend}$ mode of water. d, corresponding dispersion plot for O—H$_{bend}$ of water shows green points upper polaritonic state VP_+ and red points lower polaritonic state VP_- and dotted black line presents the O—H$_{bend}$ mode of water (with standard deviation by error bars), hollow red circles show the cavity mode position.

5 nm thick.[34] In the rest of the article we will call this ultra-thin water layer that is persistently bound to the surface of the dry sample "surface-bound water." Since even the dry sample showed resonance splitting, we estimated the width of the un-coupled plasmonic mode with optical simulations. The obtained width of ≈258 cm^{-1} shows good agreement with the experimentally measured linewidths of uncoupled off-resonance plasmonic cavities (Figures S3 and S9b, Supporting Information). Here, the surface morphology was improved using monocrystalline silver grown epitaxially on the silicon substrate[31] (Figure S2, Supporting Information), which strongly enhances the polaritonic peaks (Figure 2b) compared to the polycrystalline sample, where the splitting due to the surface-bound water is visible but less pronounced (Figure 1b). We note that the O—H bending mode at 1640 cm^{-1}, which couples with the 1st mid-IR plasmonic mode, shows no clear splitting due to surface-bound water and instead a slight shoulder appears, more closely resembling the SEIRAS effect seen with surface adsorbed CO_2 (Figures S4 and S5, Supporting Information). This is not surprising since the oscillator

strength of the O—H bending mode of water is one order of magnitude smaller than that of the O—H stretching mode.[35]

4. Vibrational Strong Coupling for 44 nm Water Layers

Open plasmonic cavities allow for spectral mapping as a function of water layer thickness all the way from bulk to surface-bound water (dry sample). To study vibrational strong coupling as a function of water layer thickness, we place a water droplet on the sample and monitor the ON resonance plasmonic cavity (P$_x$ = 1200 nm). During the measurement, the FTIR sample compartment is purged continuously with nitrogen flow under continuous monitoring of the spectrum, allowing for facile tracking of coupling and observing the Rabi splitting during the evaporation of water (**Figure 3a**). In the initial measurement, we can only probe the reflection spectrum of bulk water, which is so strong that it completely obscures the optical signature of the resonant plasmonic cavity (Figure 3b; yellow curve). As water evaporates,

**ADVANCED
SCIENCE NEWS**

www.advancedsciencenews.com

**ADVANCED
OPTICAL
MATERIALS**

www.advopticalmat.de

the constant scanning of extinction spectra shows the polaritonic peaks appear. We estimated the thickness of the water layer at each point in time by comparing the shift in the off-resonant cavity modes to simulations with different water layer thicknesses (Figure S7, Supporting Information). These measurements show that for a 44 nm water layer (blue line, Figure 3b) the polaritonic states form both in the water bending and stretching frequency region that couple with the 1st and 2nd mid-IR plasmonic modes, respectively. Here, we find a Rabi splitting energy for the O—H stretching frequency of 468 cm^{-1}, at positions $VP_+ = 3500$ cm^{-1} and $VP_- = 3032$ cm^{-1} (Figure 3b; blue curve). This splitting exceeds both the average linewidth of the corresponding cavity mode and molecular vibration for the O—H stretching band of water, fulfilling the criterion for vibrational strong coupling. The 44 nm water layer also allows the O—H bending mode to couple with the 1st plasmonic mode, resulting in a Rabi splitting of ≈300 cm^{-1} (Figure 3b; blue curve). Interestingly, this shows vibrational strong coupling of the O—H stretching and bending modes at the same time. The polaritonic peaks appearing from the bending mode are much narrower and sharper, and therefore used to examine the Rabi splitting in more detail as described below.

We perform detuning experiments with the plasmonic grating spanning a range of periodicities from $P_x = 900$ to 1400 nm. We monitored the polaritonic peaks under a constant nitrogen flow while the water gradually evaporated from the bulk to a thin layer of water (≈44 nm thick, blue line Figure 3b), and eventually to the dry sample (red line, surface-bound water remaining) enabling continuous spectral scans to probe the dispersive curve for all periodicities. This periodicity range varies the resonant frequency of the 1st mid-IR plasmonic mode from 1400–2200 cm^{-1}, targeting the bending mode of water for this detuning experiment, allowing us to demonstrate the dispersive behavior of the polaritonic states (Figure 3c). The bending mode's lower oscillator strength allows us to track the evolution of the peak splitting over a larger water thickness range where the stretching mode is completely saturated. As the water evaporates, the two polaritonic peaks from the coupled bending band become more distinct compared to the broader and more saturated stretching mode (Figure S8, Supporting Information). As the plasmonic cavity mode is tuned across the bending vibrational mode of water, the resonance clearly evolves from a single peak corresponding to the uncoupled cavity, to a split peak coming from the upper and lower polaritonic states and back to a single uncoupled cavity peak. These upper and lower polaritonic peaks are plotted as function of cavity detuning, showing the expected anti-crossing behavior of the two branches (Figure 3d). The periodicity dependence of the cavity mode is based on the measured value for the bare sample and corrected for the shift due to the water layer (Figure S7b, Supporting Information). The observed Rabi splitting energy for the polariton modes near the water bending frequency is ≈282 cm^{-1}, which is greater than the average linewidth of the molecular vibration (192 cm^{-1}) and cavity photon (≈275 cm^{-1}) on-resonance, showing that the bending mode also meets the criteria for vibrational strong coupling.

For a final confirmation of vibrational strong coupling of the 44 nm water layer to our plasmonic cavities, we also demonstrate the concentration dependent experiment of water by changing the ratio of H_2O to D_2O. D_2O has two major bands: the O—D stretching is at 2500 cm^{-1} and the O—D bending is at 1250 cm^{-1}.

It also contains an H—O—D bending mode arising from some water contamination in the D_2O solvent, which overlaps with the lower polaritonic peak of the bending mode, making it necessary to use the O—H stretching mode for these water concentration experiments (Figure S9a, Supporting Information). By varying the concentration of water in D_2O from 1% to 100%, the splitting energy of the polaritons in the O—H stretching region changes from 216 to 468 cm^{-1} (**Figure 4a**) and follows the expected square root behavior with concentration[35] (Figure 4b). We observe that at low concentrations of water, the system is not quite in vibrational strong coupling; it crosses into the strong coupling regime at ≈10% water. These mixed H_2O/D_2O experiments exhibit a few features that deserve further comment. First, even in the pure D_2O solution, we still observe a clear water peak, not only in the measurement of the 44 nm liquid layer, but also in the bulk measurement. This comes from a 1% water impurity in the D_2O (as reported by the chemical producer), which is consistent with our bulk measurements. Nevertheless, even after extended periods of time in 99% D_2O, this surface water signal does not disappear or even decrease, suggesting that there may be some trapped H_2O at the interface between the silicon and the silver or a tightly bound surface-adsorbed H_2O layer that is not labile in D_2O. It is also possible that during evaporation, the remaining water molecules isotope exchange with H_2O in air, with the result that the residual surface-bound deuterated water molecules largely become H_2O molecules.

The trapped or persistently bound surface water gives an expected splitting energy of 200 cm^{-1} (y-intercept in Figure 4b), and this splitting energy is nearly identical to that of the dry cavity observed in Figure 2b (202 cm^{-1}). It is reasonable to assume that the water layer that remains even after the cavity has been completely dried (also under vacuum annealing), is the same as the layer that remains in pure (99%) D_2O. Raman measurements on the bare samples provide additional evidence for the presence of trapped or persistently bound surface water molecules (Figure S10, Supporting Information). There are several studies showing that even at very low relative humidity (< 15%) and under vacuum (1.2 Torr) several monolayers up to several nanometers of water can remain on silicon oxide and metal surfaces.[34,36] Furthermore, as this water layer becomes thicker, it develops a strong surface potential, indicating water dipole alignment.[36] This aligned surface water can help improve coupling to the plasmonic mode, since proper dipole alignment between the plasmonic mode and the water dipoles is necessary for vibrational strong coupling. This dipole alignment at the surface may help explain our observation that we are on the cusp of vibrational strong coupling even with the ultrathin water layer that remains persistently bound to the surface after vacuum annealing or extended contact with 99% D_2O. Our ongoing studies on these systems are investigating the water orientation and if it can be influenced by the plasmonic resonance frequency.

5. Conclusion

There have been several attempts to produce vibrational strong coupling for water molecules that can accelerate or retard a chemical process in closed cavities[6,37–39] and to understand the nature of water[35,40,41] but all of those studies probed bulk water, rather than surface water, and therefore are not relevant for
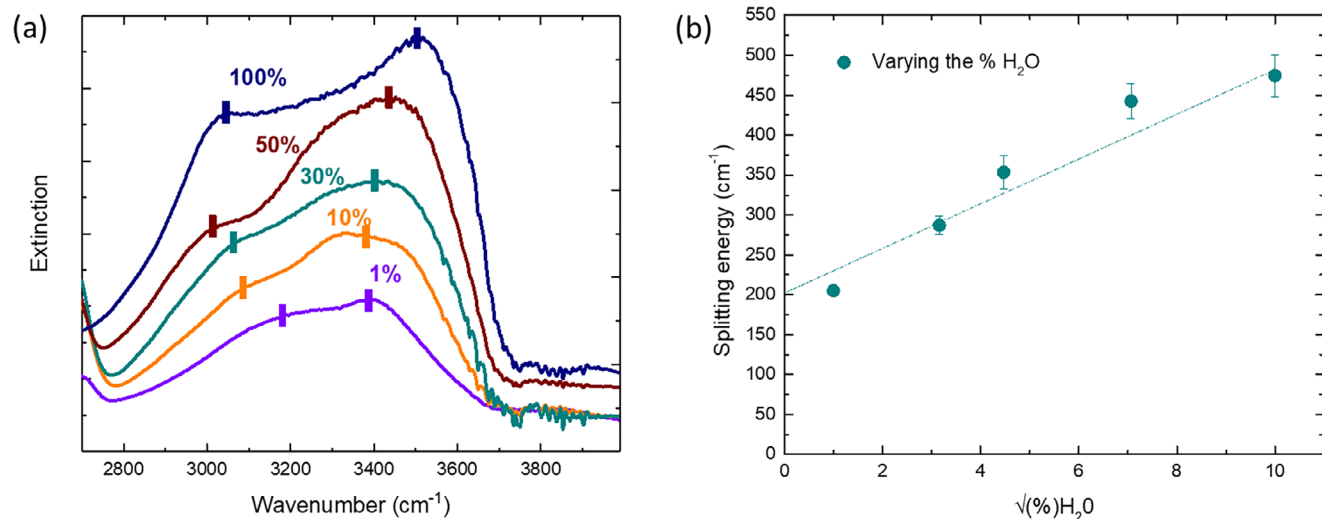
e01890 (5 of 7)

**ADVANCED
SCIENCE NEWS**

www.advancedsciencenews.com

**ADVANCED
OPTICAL
MATERIALS**

www.advopticalmat.de

Figure 4. a) Varying the concentration of H_2O by adding D_2O from 1% of H_2O (blue curve) to 100% of H_2O (blue curve), each concentration measurement assumes a thin layer of water with the thickness of ~44 nm; shows the shifting of polaritonic peaks. b) corresponding plot for the square root of water percentage with Rabi splitting (with standard deviation by error bars); that follow by the linear fit.

tuning chemical reactivity in surface-catalyzed reactions. We have fabricated plasmonic cavities that can couple with ultrathin water layers, leading to vibrational strong coupling in both the stretching and bending modes for 44 nm water layers. In the stronger bending mode, clear peak splitting is seen that is just below the threshold for vibrational strong coupling even in dry samples where the surface-bound water layer is estimated only to be between a few monolayers and a few nanometers thick. This result opens up the possibility to use vibrational strong coupling to tune catalytic reactions at surfaces, which comprise the vast majority of industrial chemistry. In particular, this demonstration with water has direct implications for aqueous electrocatalysis, with relevance for critically important reactions for the sustainable energy transition such as water-splitting and CO_2 reduction. Beyond this clear industrial relevance, water is one of the most well-studied solvents and participates in many reactions as either an intermediate or reactant. This study provides a pathway for greater fundamental understanding of vibrational strong coupling effects, for example by controlling the orientation of water molecules at an electrochemical interface and studying the resulting effects on Rabi splitting and chemical reactions.

6. Experimental Section

Finite-Difference Time-Domain (FDTD) Simulations: The simulations were performed using Lumerical to obtain the electric-field enhancement profile. A 3D structure of nanogroove with a trapezoidal cross-section was implemented in a silver film. More details can be found in Section S1 (Supporting Information).

Plasmonic Cavities Fabrication: The nanogrooves were fabricated on a 12 × 12 mm silicon substrate (p-type, boron-doped ⟨100⟩, purchased from Siegert Wafer GmbH). A 60 nm thick SiO_2 hard mask was grown using rapid thermal annealing (AnnealSys AS-One 100). For lithography, poly methyl methacrylate (PMMA 495 A8) was spin-coated to a thickness of ≈300 nm (spin coater- Suss MicroTec -Delta 80). An array of nanogrooves, each 200 nm wide and 4 μm long was patterned over a 250 × 250 μm² area using electron beam lithography (Raith Voyager). Each array had a

different periodicity and was separated by 1 mm, as shown in Figure 1a. The periodicity has been varied for one direction (p_x) from 500 to 4000 nm, and the other (p_y) was kept constant at 5000 nm. After resist development, the nanogrooves were first etched using reactive ion etching (RIE- Plasma 80 Plus) with CHF_3/Ar to etch the SiO_2. For the selective RIE of Si, the nanogrooves were etched with $Cl_2/HBr/O_2$ (Oxford Instruments Plasma Technology- NGP 100 Cobra), which gives the resulting depth of the nanogrooves. The sample was placed for resist ashing in oxygen plasma (Diener Electronic Plasma Surface Technology- Pico) and finally, the hard mask (SiO_2) was completely removed using an HF vapor etcher (SPTS KLA- Primaxx® uEtch). A 100 nm of polycrystalline silver film was deposited (0.05 nm sec^{-1}) on Si nanogrooves using electron beam physical vapor deposition system (Polyteknik - Flextura M508 E). For the monocrystalline silver epitaxial deposition, the native oxide on the Si nanogrooves was removed using the HF vapor etcher and then the substrate was immediately placed in the e-beam vapor deposition chamber under high vacuum. For single monocrystalline silver film deposition requires a three-step process: i) silver seed crystal islands of ≈5 nm were grown on the substrate at a substrate temperature of 350 °C and base pressure of $1.38e^{-6}$ mbar. ii) cool the chamber to room-temperature and deposited a 95 nm silver film on the seeds. iii) the film was annealed at 450 °C in the same vacuum chamber.

Microscopy: The quality and uniformity of the silver film surface were investigated using scanning electron microscopy (SEM, FEI Verios 460) operated at an accelerating voltage of 5 kV and a beam current of 100 pA. The surface morphology of the film was characterized by an atomic force microscope (AFM- Bruker dimension icon) with SCANASYST-AIR probe. Nanoscope software was used to analyze the AFM images. To confirm the crystallographic orientation of the deposited silver film, electron backscattered diffraction (EBSD) was performed using an EDAX Clarity system with a Timepix detector from Amsterdam Scientific Instruments (ASI). Further details can be found in Section S3 (Supporting Information).

Fourier-Transform Infrared (FTIR) Microscope: Infrared (IR) spectra of the nanogroove arrays were recorded in reflection mode using a 15× objective (numerical aperture = 0.4, incident angle range ± 23.6°) with an IR microscope (Bruker Hyperion) coupled to an FTIR spectrometer (Bruker Vertex 80v). To minimize atmospheric influences of CO_2 and H_2O vapors in the IR microscope the chamber was continuously purged with nitrogen. Measurements were carried out in reflection mode with a resolution of 4 cm^{-1} and 32 scans. FTIR spectra were acquired by collecting the signal from the nanogroove arrays and correcting the background signal from a bare silver mirror under the same conditions. A drop of water was placed

on the arrays, and the constant nitrogen flow inside the chamber allowed the water to evaporate slowly, until bulk water becomes a few monolayers. Continuous spectral scanning enabled the probing of the polaritonic peaks. Deionized (DI) water obtained from a laboratory-grade purification system was used for all experiments. Deuterium oxide (D_2O, CAS No. 7789-20-0) was obtained from Sigma–Aldrich.

Supporting Information

Supporting Information is available from the Wiley Online Library or from the author.

Conflict of Interest

The authors declare no conflict of interest.

Data Availability Statement

The data that support the findings of this study are available from the corresponding author upon reasonable request.

Keywords

nanogrooves, plasmonic cavities, polaritonic chemistry, vibrational strong coupling

[1] A. Thomas, J. George, A. Shalabney, M. Dryzhakov, S. J. Varma, J. Moran, T. Chervy, X. Zhong, E. Devaux, C. Genet, J. A. Hutchison, T. W. Ebbesen, *Angew. Chem. Int. Ed.* **2016**, *55*, 11634.

[2] X. Li, A. Mandal, P. Huo, *J. Phys. Chem. Lett.* **2021**, *12*, 6974.

[3] A. Thomas, E. Devaux, K. Nagarajan, G. Rogez, M. Seidel, F. Richard, C. Genet, M. Drillon, T. W. Ebbesen, *Nano Lett.* **2021**, *21*, 4365.

[4] K. Hirai, H. Uji-i, *Chem. Lett.* **2021**, *50*, 727.

[5] J. Lather, P. Bhatt, A. Thomas, T. W. Ebbesen, J. George, *Angew. Chem. Int. Ed.* **2019**, *58*, 10635.

[6] T. Fukushima, S. Yoshimitsu, K. Murakoshi, *J. Am. Chem. Soc.* **2022**, *144*, 12177.

[7] R. M. A. Vergauwe, A. Thomas, K. Nagarajan, A. Shalabney, J. George, T. Chervy, M. Seidel, E. Devaux, V. Torbeev, T. W. Ebbesen, *Angew. Chem.* **2019**, *58*, 15324.

[8] J. Singh, P. Garg, R. V. Anand, J. George, *Chem. Eur. J.* **2024**, *30*, 202400607.

[9] Y. Pang, A. Thomas, K. Nagarajan, R. M. A. Vergauwe, K. Joseph, B. Patrahau, K. Wang, C. Genet, T. W. Ebbesen, *Angew. Chem. Int. Ed.* **2020**, *59*, 10436.

[10] A. Thomas, L. Lethuillier-Karl, K. Nagarajan, R. M. A. Vergauwe, J. George, T. Chervy, A. Shalabney, E. Devaux, C. Genet, J. Moran, T. W. Ebbesen, *Science* **2019**, *363*, 615.

[11] A. Sau, K. Nagarajan, B. Patrahau, L. Lethuillier-Karl, R. M. A. Vergauwe, A. Thomas, J. Moran, C. Genet, T. W. Ebbesen, *Angew. Chem. Int. Ed.* **2021**, *60*, 5712.

[12] T. W. Ebbesen, *Acc. Chem. Res.* **2016**, *49*, 2403.

[13] T. E. Li, B. Cui, J. E. Subotnik, A. Nitzan, *Annu. Rev. Phys. Chem.* **2022**, *73*, 43.

[14] K. Nagarajan, A. Thomas, T. W. Ebbesen, *J. Am. Chem. Soc.* **2021**, *143*, 16877.

[15] J. George, A. Shalabney, J. A. Hutchison, C. Genet, T. W. Ebbesen, *J. Phys. Chem. Lett.* **2015**, *6*, 1027.

[16] J. George, T. Chervy, A. Shalabney, E. Devaux, H. Hiura, C. Genet, T. W. Ebbesen, *Phys. Rev. Lett.* **2016**, *117*, 153601.

[17] Z. W. She, J. Kibsgaard, C. F. Dickens, I. Chorkendorff, J. K. Nørskov, T. F. Jaramillo, *Science* **2017**, *355*, aad4998.

[18] E. Oksenberg, I. Shlesinger, G. Tek, A. F. Koenderink, E. C. Garnett, *Adv. Funct. Mater.* **2023**, *33*, 2211154.

[19] Y. Yang, R. Chikkaraddy, Q. Lin, D. D. A. Clarke, D. Wigger, J. J. Baumberg, O. Hess, *Nano Lett.* **2024**, *24*, 238.

[20] R. Chikkaraddy, B. De Nijs, F. Benz, S. J. Barrow, O. A. Scherman, E. Rosta, A. Demetriadou, P. Fox, O. Hess, J. J. Baumberg, *Nature* **2016**, *535*, 127.

[21] W. Chen, P. Roelli, H. Hu, S. Verlekar, S. P. Amirtharaj, A. I. Barreda, T. J. Kippenberg, M. Kovylina, E. Verhagen, A. Martínez, C. Galland, *Science* **2021**, *374*, 1264.

[22] G. E. Akinoglu, J. A. Hutchison, *ACS Appl. Opt. Mater.* **2023**, *1*, 771.

[23] M. Mondal, A. Semenov, M. A. Ochoa, A. Nitzan, *J. Phys. Chem. Lett.* **2022**, *13*, 9673.

[24] W. Wan, X. Yang, J. Gao, *Opt. Express* **2016**, *24*, 12367.

[25] M. Hertzog, B. Munkhbat, D. Baranov, T. Shegai, K. Börjesson, *Nano Lett.* **2021**, *21*, 1320.

[26] R. Arul, K. Menghrajani, M. S. Rider, R. Chikkaraddy, W. L. Barnes, J. J. Baumberg, *Phys. Rev. Lett.* **2023**, *131*, 126902.

[27] K. S. Menghrajani, G. R. Nash, W. L. Barnes, *ACS Photonics* **2019**, *6*, 2110.

[28] F. Verdelli, Y. C. Wei, K. Joseph, M. S. Abdelkhalik, M. Goudarzi, S. H. C. Askes, A. Baldi, E. W. Meijer, J. Gomez Rivas, *Angew. Chem., Int. Ed.* **2024**, *63*, 202409528.

[29] Z. T. Brawley, S. Pannir-Sivajothi, J. E. Yim, Y. R. Poh, J. Yuen-Zhou, M. Sheldon, *Nat. Chem.* **2025**, *17*, 439.

[30] P. A. Thomas, W. J. Tan, H. A. Fernandez, W. L. Barnes, *Nano Lett.* **2020**, *20*, 6412.

[31] I. A. Rodionov, A. S. Baburin, A. R. Gabidullin, S. S. Maklakov, S. Peters, I. A. Ryzhikov, A. V. Andriyash, *Sci. Rep.* **2019**, *9*, 12232.

[32] C. Huck, J. Vogt, M. Sendner, D. Hengstler, F. Neubrech, A. Pucci, *ACS Photonics* **2015**, *2*, 1489.

[33] F. Neubrech, C. Huck, K. Weber, A. Pucci, H. Giessen, *Chem. Rev.* **2017**, *117*, 5110.

[34] J. Freund, J. Halbritter, J. K. H. Hörber, *Microsc. Res. Tech.* **1999**, *44*, 327.

[35] T. Fukushima, S. Yoshimitsu, K. Murakoshi, *J. Phys. Chem. C* **2021**, *125*, 25832.

[36] A. Verdaguer, C. Weis, G. Oncins, H. Bluhm, M. Salmero, *Langmuir* **2007**, *23*, 9699.

[37] R. M. A. Vergauwe, A. Thomas, K. Nagarajan, A. Shalabney, J. George, T. Chervy, M. Seidel, E. Devaux, V. Torbeev, T. W. Ebbesen, *Angew. Chem. Int. Ed.* **2019**, *58*, 15324.

[38] T. Fukushima, S. Yoshimitsu, K. Murakoshi, *Chem. Sci.* **2023**, *14*, 11441.

[39] K. Gu, Q. Si, N. Li, F. Gao, L. Wang, F. Zhang, *ACS Photonics* **2023**, *10*, 1633.

[40] T. E. Li, J. E. Subotnik, A. Nitzan, *Proc. Natl. Acad. Sci.* **2020**, *117*, 18324.

[41] A. Kadyan, M. P. Suresh, B. Johns, J. George, *ChemPhysChem* **2024**, *25*, 202300560.